

## Covariations of Sea Surface Temperature and Wind over the Kuroshio and Its Extension: Evidence for Ocean-to-Atmosphere Feedback\*

MASAMI NONAKA

*International Pacific Research Center, University of Hawaii at Manoa, Honolulu, Hawaii, and  
Frontier Research System for Global Change, Yokohama, Japan*

SHANG-PING XIE

*International Pacific Research Center, and Department of Meteorology, University of Hawaii at Manoa, Honolulu, Hawaii*

(Manuscript received 8 July 2002, in final form 17 October 2002)

### ABSTRACT

Satellite microwave measurements are analyzed, revealing robust covariability in sea surface temperature (SST) and wind speed over the Kuroshio Extension (KE) east of Japan. Ocean hydrodynamic instabilities cause the KE to meander and result in large SST variations. Increased (reduced) wind speeds are found to be associated with warm (cold) SST anomalies. This positive SST–wind correlation in KE is confirmed by in situ buoy measurements and is consistent with a vertical shear adjustment mechanism. Namely, an increase in SST reduces the static stability of the near-surface atmosphere, intensifying the vertical turbulence mixing and bringing fast-moving air from aloft to the sea surface.

South of Japan, the Kuroshio is known to vary between nearshore and offshore paths. These paths are very persistent and can last for months to years. As the Kuroshio shifts its path, coherent wind changes are detected from satellite data. In particular, winds are high south of Tokyo when the Kuroshio takes the nearshore path while they are greatly reduced when this warm current leaves the coast in the offshore path.

The positive SST–wind correlation over the strong Kuroshio Current and its extension is opposite to the negative one often observed in regions of weak currents such as south of the Aleutian low. The latter correlation is considered to be indicative of atmosphere-to-ocean forcing.

### 1. Introduction

It has been known for quite some time that basin-scale North Pacific SST variability is significantly correlated with wind velocity both at the sea surface and aloft (e.g., Namias and Cayan 1981). Positive (negative) SST anomalies (SSTAs) are often found in winter to be collocated with decreased (increased) speed of prevailing winds (Wallace et al. 1990). This negative SST–wind correlation is considered by some as indicative of atmospheric forcing of the ocean (Frankignoul 1985) by means of surface latent and sensible heat flux (e.g., Cayan 1992; Alexander et al. 2002). The search for oceanic feedback into the atmosphere, on the other hand, has not yielded conclusive evidence in the extratropics yet because of a high level of weather noise on one hand

and too short data records on the other. Czaja and Frankignoul (1999) is an example of recent diagnostic attempts whose results hint at an oceanic feedback. General circulation models are still in disagreement among themselves with regard to whether and how the atmosphere responds to extratropical SST anomalies (Robinson 2000).

Oceanic fronts may offer unique opportunities to study ocean-to-atmosphere feedback. Those fronts are generally associated with strong ocean currents, whose hydrodynamic instabilities can cause the fronts to meander and SST to vary. In fact, buoy observations on the Pacific equatorial front ( $\sim 2^\circ\text{N}$ ) have captured such ocean–atmosphere covariability induced by tropical instability waves (TIWs; Hayes et al. 1989). In general, however, oceanic fronts are not well monitored by in situ measurements because they tend to be located in remote oceans. Recent advance in satellite microwave remote sensing is revolutionizing how we observe the oceans and reveals structures of oceans and their interaction with the atmosphere in detail never possible before (Wentz et al. 2000; Xie et al. 2001; Liu 2002). For example, new satellite observations reveal a long shadow of the Hawaiian Islands in the Pacific Ocean and

---

\* International Pacific Research Center Contribution Number 189 and School of Ocean and Earth Sciences Contribution Number 6097.

---

*Corresponding author address:* Dr. Masami Nonaka, International Pacific Research Center, University of Hawaii at Manoa, 2525 Correa Road, Honolulu, HI 96822.  
E-mail: mnonaka@hawaii.edu

atmosphere that is triggered by the steady trade winds impinging upon the high mountains on the islands (Xie et al. 2001).

*European Remote Sensing Satellite-1 (ERS-1)* captures wind fluctuations associated with TIWs in the eastern equatorial Pacific, demonstrating the utility of satellite scatterometers for studying large-scale ocean–atmosphere interaction (Xie et al. 1998). TIW-induced atmospheric variability has been mapped in detail by using high-resolution scatterometer measurements on the National Aeronautics and Space Administration’s Quick Scatterometer (QuikSCAT) satellite (Liu et al. 2000; Chelton et al. 2001; Hashizume et al. 2001), sometimes in combination with other independent satellite data. These observational studies reveal a positive correlation between SST and surface wind speed, just opposite to that often observed in the extratropical central North Pacific in winter.

Our focus here is the Kuroshio Current south of Japan and its extension to the east. Being the western boundary current of the subtropical North Pacific, the intense Kuroshio flows along the south coast of Kyushu and Shikoku Islands, then separates from the Japanese coast and continues eastward as an inertial jet. This eastward jet, called the Kuroshio Extension (KE), separates warmer subtropical water in the south from colder subpolar water in the north and appears as a sharp SST front, in which SST can change as much as  $10^{\circ}\text{C}$  in 100 km. The jet is highly unstable and accompanied by large meanders and energetic pinched-off eddies (Mizuno and White 1983), readily visible from satellite observations (Toba and Murakami 1998). The KE region has the highest level of eddy kinetic energy in the Pacific Ocean (Wyrki et al. 1976; Qiu 2002). Like TIWs on the equatorial front, strong eddy activity on the KE gives rise to large SST variations on subseasonal timescales, which conceivably further lead to coherent atmospheric covariability.

The present study investigates the wind response to SST variability induced by the meandering Kuroshio and its extension. We take advantage of new microwave measurements on the QuikSCAT and Tropical Rainfall Measurement Mission (TRMM) satellites, which see through most of clouds except those with sizable precipitation. Buoy observations east of Japan are used to validate the findings from satellite observations. The KE area is also the major region of atmospheric cyclogenesis in the North Pacific, where wind speed can vary from a few meters per second under calm conditions to over  $30\text{ m s}^{-1}$  in major storms. Such strong weather disturbances pose a challenge for detecting much weaker SST effect. Using several techniques to be described, we detect SST-induced wind signals that are robustly correlated with SSTAs.

The rest of this paper is organized as follows. Section 2 described the datasets. Atmospheric response is investigated using satellite data in section 3, and with buoy data in section 4. Section 5 investigates the air–sea cou-

pling over the Kuroshio region south of Japan. Section 6 is a summary.

## 2. Data

### a. Satellite measurements

We combine and analyze the surface wind and SST observations of several satellite sensors on different platforms to extend the observation periods or gain high resolution in space and time. This multisensor approach will give us more confidence in the results if these independent measurements converge and give physically consistent pictures.

The TRMM Microwave Imager (TMI) measures SST at a  $0.25^{\circ}$  horizontal resolution and covers the whole Tropics and subtropics within  $38^{\circ}$  latitudes every 3 days. Here we use a weekly mean product on a  $0.25^{\circ}$  grid for a period from December 1997 to May 2002. We use the Advanced Very High Resolution Radiometer (AVHRR) Pathfinder monthly mean SST product based on infrared sensors (Vazquez et al. 1998) for periods before the TMI observations. While the AVHRR offers much higher resolutions in time and space, we use a monthly product on a coarse  $0.5^{\circ}$  grid to increase the sampling size and minimize the effect of clouds that are frequently found in the KE region.

QuikSCAT measures surface wind velocity covering more than 90% of the world ocean on a daily basis (Liu et al. 2000). We use a weekly mean QuikSCAT product available on a  $0.5^{\circ}$  grid for August 1999 to April 2002. A monthly mean ERS wind velocity dataset on a  $1^{\circ}$  grid is used from September 1991. For scalar wind speed, we use the same TMI dataset for recent years and a monthly mean Special Sensor Microwave Imager (SSM/I) product on a  $1^{\circ}$  grid from January 1987.

For the dynamic variable of sea surface height (SSH), we use a dataset that merges observations by the TOPEX/Poseidon (T/P) and ERS altimeters on a  $0.5^{\circ}$  grid and 10-day time interval (Ducet et al. 2000).

### b. In situ observations

As ground truth, we use in situ measurements of SST, air temperature, and surface wind velocity at buoys operated by the Japan Meteorological Agency. Such buoy measurements were available in the northern part of the Kuroshio Extension region at  $38.5^{\circ}\text{N}$ ,  $145.5^{\circ}\text{E}$  (from September 1980 to November 1986) and  $36.7^{\circ}\text{N}$ ,  $145.7^{\circ}\text{E}$  (from April 1987 to June 1991). There are extensive periods of missing data, and continuous time series are obtained in only four winter-to-spring seasons as will be analyzed in section 4. We use the National Centers for Environmental Prediction–National Center for Atmospheric Research (NCEP–NCAR) reanalysis data (Kalnay et al. 1996) to remove large-scale atmospheric variability from the buoy data with a procedure to be described.

### 3. Kuroshio Extension

Figure 1 (top) shows AVHRR SST in KE averaged for January–March 1997 (contours). Even on this seasonal mean, there are strong zonally oriented fronts: one in 35°–37°N and one farther to the north. These fronts meander at typical zonal wavelengths of about 1000 km (Tai and White 1990; Qiu et al. 1991). These meanders are ubiquitous and caused by dynamic instabilities of the KE jet (Hurlburt et al. 1996; Qiu 1995). Surface wind speed appears to vary with these meanders of the SST fronts; the correlation is especially clear on the southern front. For example, the trough of the front around 158°E, 35°N is associated with a local reduction of wind speed, and the ridge to the east with a wind speed increase (color shade). Since the westerlies prevail in this region, this corresponds to a westerly acceleration over the ridge (positive SSTAs) and vice versa.

To isolate these meanders with typical wavelengths of 1000 km, we remove from the original data 10° running-means in the zonal direction. As in the case of TIWs (Hashizume et al. 2001), this high-pass zonal filter effectively removes seasonal cycle and other larger-scale variations. Hereafter in this section, we call the high-pass-filtered fields anomalies. The results are not sensitive to the choice of the length scale for the zonal filter if it is larger than 6°.

#### a. Time–longitude structure

Figure 2 shows the longitude–time sections of so-defined anomalies of SSH, SST, and wind speed at 35°N, which is the approximate axis of the KE. Large SSH anomalies (SSHAs) of up to 0.6 m are present, showing a general tendency to propagate westward, with typical timescales of a few months (Fig. 2, left). Somehow, both the time- and zonal scales of the KE meanders become much smaller west of 155°E. The speed of westward propagation varies not only with longitude as pointed out by the previous studies (Tai and White 1990; Qiu et al. 1991), but also with time. For this reason, we do not attempt to determine the propagation speed.

The meanders of the KE front are associated with pronounced SSTAs that propagate westward together with SSHAs (Fig. 2, middle). To facilitate comparison among the three parts of Fig. 2, we draw a few approximate equal-phase lines in each panel. Visual examination indicates that SSTAs and SSHAs are roughly in phase, consistent with a previous study (Qiu et al. 1991). This in-phase relationship between SST and SSH may be due to the deep mixed layer there, the time lag between the maximum thermal advection and maximum SSTA, or both. (Temperature anomalies of a deep mixed layer induce large changes in SSHA. Maximum meridional heat transport takes place with the SSHA maximum to the east and minimum to the west, but the resultant maximum SST occurs a quarter period later, coinciding with the SSH maximum.)

More remarkably, the same westward propagation is clearly visible also in wind speed (Fig. 2, right). Comparison of SST and wind speed using the phase lines as reference indicates that they are in phase, with increased wind speed over positive SSTAs, confirming what we inferred from Fig. 1. Local SST–wind speed correlation averaged in 145°E–180° for December–May of 1998–2002 amounts to 0.68. While weather disturbances are indeed very strong, they have larger zonal scale and hence were removed efficiently by our zonal filter.

Chelton et al. (2001) find that TMI-derived SST has a small bias relative to buoy measurements, which varies from positive to slightly negative as wind speed increases (their Fig. 2b). This wind speed dependence of TMI SST bias is opposite to the positive SST–wind correlation we are reporting in the KE region, suggesting that meander-induced wind speed variability is unlikely an artifact of satellite sensor bias. Unaware of any other mechanisms for SST and wind speed to show a consistent tendency of westward propagation, we attribute these traveling SST anomalies to KE's dynamic instabilities, which further induce wind speed variability.

#### b. Seasonality

Figure 3 shows area-mean variance for high-pass-filtered SSH, SST, and wind speed fields as a function of time. While previous studies using the short *Geosat* record suggests that the SSH variance increases in the summer to fall (Tai and White 1990), it does not have obvious seasonality in the 3.5-yr period of our analysis (Fig. 3, top). By contrast, SST variance shows a seasonal maximum in each of five winters in TMI observations (Fig. 3, middle). This SST seasonality is probably due to seasonal variability in the strength of the SST front along KE. Shallow mixed layers in summer discriminate against advective heat fluxes and favor a dominance of the surface heat fluxes in the surface heat budget. Conversely, deep mixed layers favor advective tendencies. In response to current variability with seasonally constant amplitudes, SST would display stronger variability in winter with a sharper SST front. A deeper mixed layer in winter may also play a role, allowing larger lateral heat transport by variable currents (Tomita et al. 2002). Wind speed variance shows a similar tendency of winter increase (Fig. 3, bottom), consistent with the notion that wind and SST variability is coupled.

#### c. Spatial structure

There are two known mechanisms for surface wind adjustment to SST changes. Winds are generally stronger upward away from the sea surface. An increase in SST reduces the static stability of the near-surface atmosphere and intensifies the vertical mixing. This brings faster wind aloft to the surface, resulting in a wind acceleration there. In addition to this vertical mixing

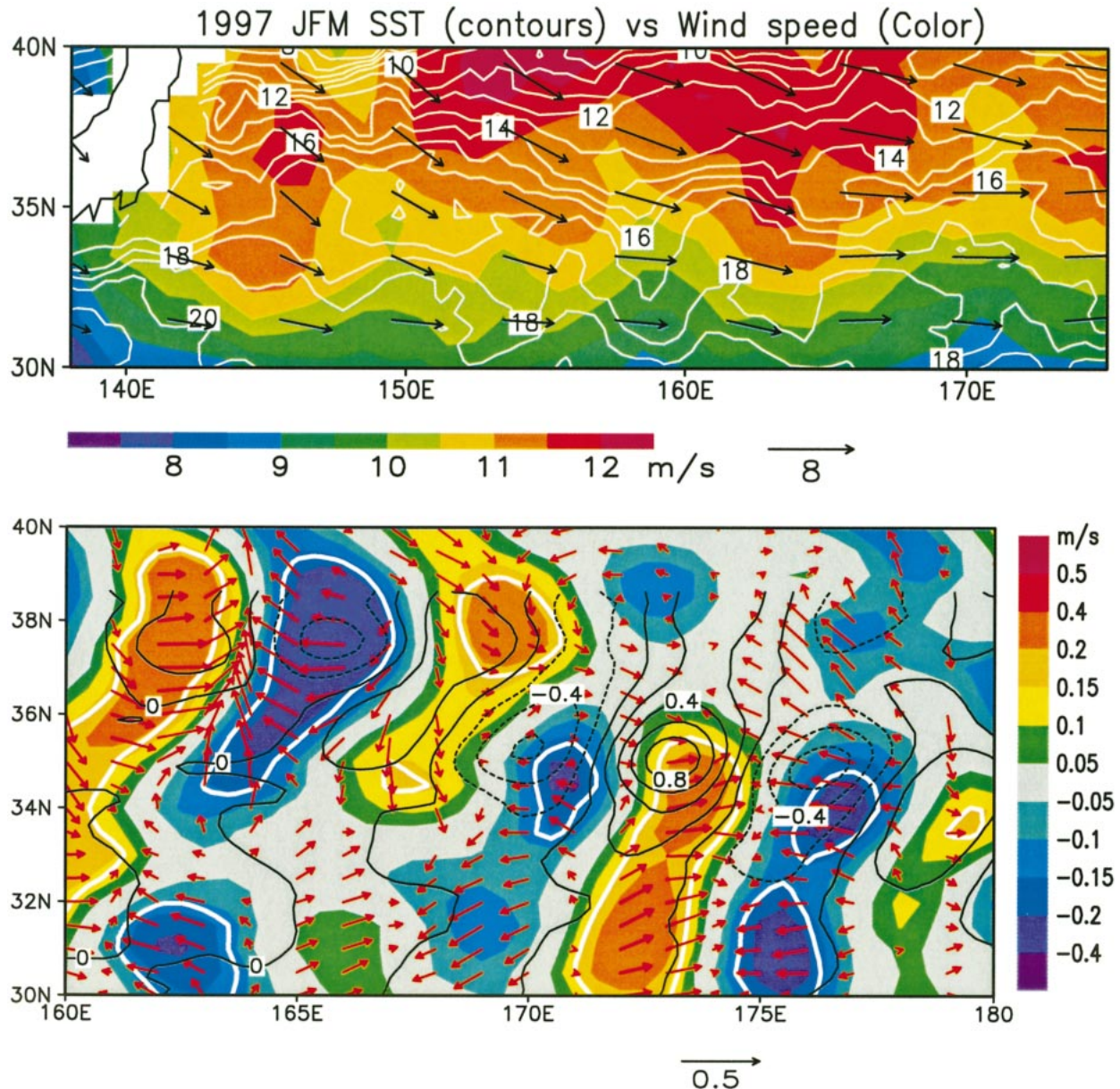


FIG. 1. (top) AVHRR SST (white contours), ERS surface wind velocity vectors and scalar speed (shaded), averaged for Jan–Mar 1997. Contour intervals are  $1^{\circ}\text{C}$  for SST and  $0.5\text{ m s}^{-1}$  for wind speed. (bottom) Composite regression fields of TMI SST (contours), QuikSCAT wind speed (color shaded in  $\text{m s}^{-1}$ ), and wind velocity vectors ( $\text{m s}^{-1}$ ) upon the SST time series of 1999–2002 in  $35^{\circ}\text{N}$ ,  $168^{\circ}\text{--}178^{\circ}\text{E}$ , in winter (Dec–May). Contour intervals for SST are  $0.2^{\circ}\text{C}$ . In region enclosed by the white contours, the wind speed regression exceeds the 95% confidence level. See text for the regression procedures.

mechanism, the SST increase warms up the boundary layer air, forming a low in the sea level pressure (SLP) field that can induce wind anomalies. The relative importance of these two mechanisms can be inferred by examining the horizontal structure of SST and surface wind speed anomalies. The vertical mixing leads to in-phase covariability while the SLP mechanism leads to a significant phase difference between SST and wind speed— $90^{\circ}$  near the equator (Hayes et al. 1989). See Hashizume et al. (2002) for a review.

To map the spatial structure of SST–wind covariability, we perform the following regression analysis. First, we compute the regression coefficient fields for TMI SST, QuikSCAT wind velocity, and scalar speed upon a reference SST time series taken at a grid point at  $35^{\circ}\text{N}$  between  $168^{\circ}\text{--}178^{\circ}\text{E}$ , a zonal span with large SST variance. The calculation is repeated with each grid point in the zonal span as the reference. A total of 21 sets of regression fields (one for every  $0.5^{\circ}$  in longitude) are obtained, which are then averaged by matching the

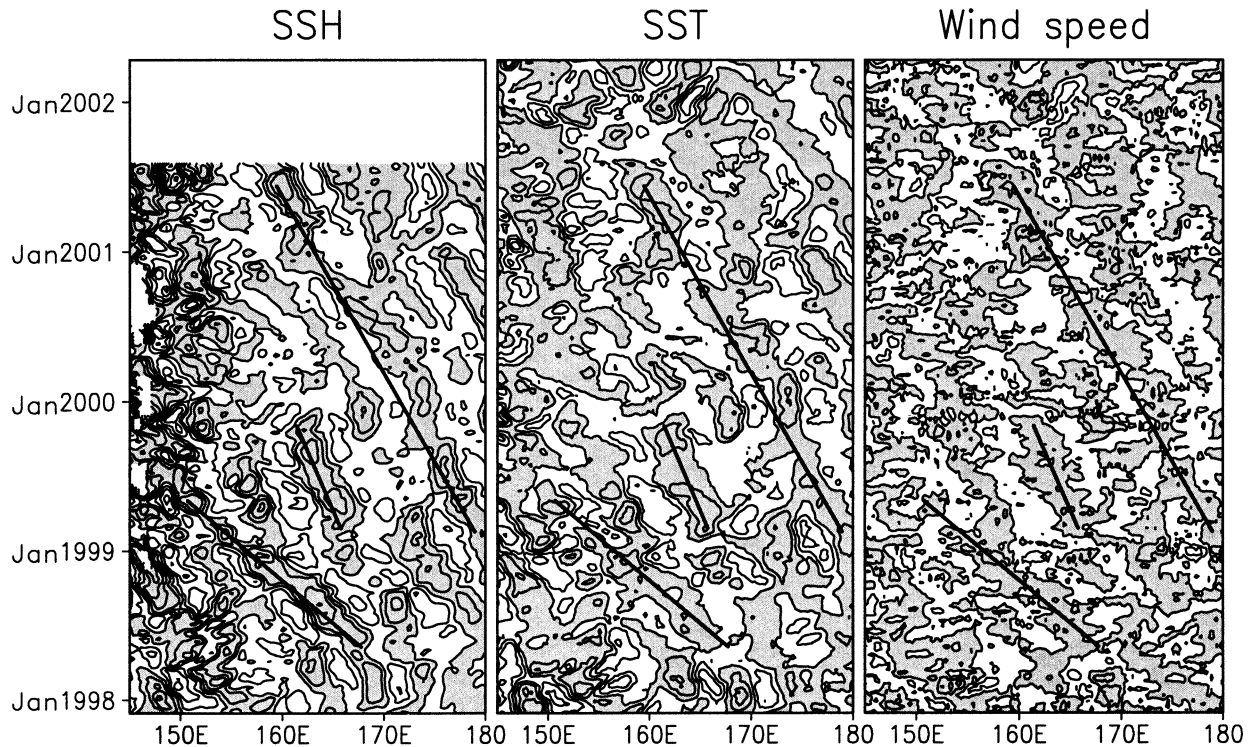


FIG. 2. Longitude–time sections of high-pass zonally filtered (left) SSH, (middle) SST, and (right) surface wind speed along  $35^{\circ}\text{N}$ , smoothed with 3-week running mean. For both SST and wind speed, weekly TMI dataset is used. Contour intervals for SSH, SST, and wind speed are 20 cm,  $1^{\circ}\text{C}$ , and  $1\text{ m s}^{-1}$ , respectively. Positive values are shaded. (left) Three thick, black lines denote constant phase lines for various westward-propagation speeds, and are repeated in other panels to facilitate phase comparison among anomalies of SSH, SST, and wind speed.

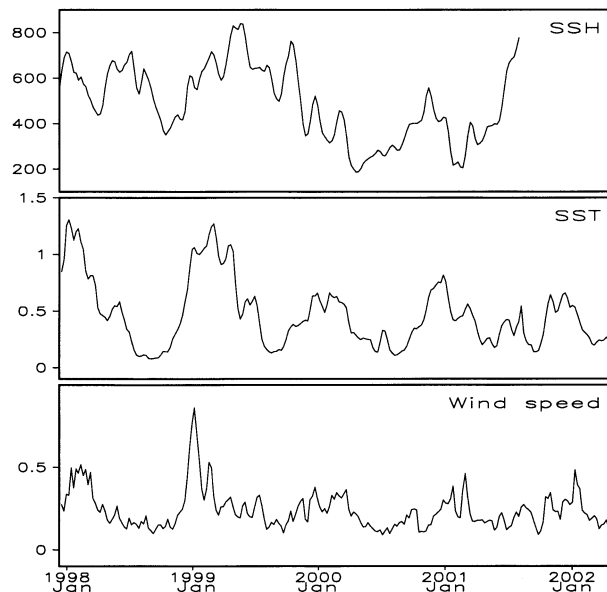


FIG. 3. Time series of variances of high-pass zonally filtered (top) SSH, (middle) SST, and (bottom) wind speed, averaged in the KE region ( $33^{\circ}\text{--}37^{\circ}\text{N}$ ,  $145^{\circ}\text{E--}180^{\circ}$ ). Three-week running means are used to estimate the variance. Units are  $\text{cm}^2$ ,  $^{\circ}\text{C}^2$ , and  $\text{m}^2\text{ s}^{-2}$  for SSH, SST, and wind speed, respectively.

reference grid points onto  $35^{\circ}\text{N}$ ,  $173^{\circ}\text{E}$ . Only data for the colder half year (December–May) of 1999–2002 are used, when both the SST and wind variances are large.

Figure 1 (bottom) shows the resultant composite regression fields that reveal coherent wavelike patterns lining up in the zonal direction. SST and wind speed anomalies are roughly in phase, with an acceleration of the prevailing westerlies (Fig. 1, top) over positive SSTAs. This in-phase relation suggests that the vertical mixing is the dominant mechanism for surface wind adjustment. The in-phase relation is not perfect, however, suggesting a possibility that some other mechanisms such as the SLP gradient driving also have an influence. A more accurate phase determination requires longer data records.

#### 4. Analysis of buoy data

Here we analyze Japan Meteorological Agency buoy observations east of Japan and investigate whether the SST–wind correlation holds. To remove seasonal variations and high-frequency weather disturbances, a band-pass filter with half power at 9 and 91 days is applied. A comparison of SLP, wind speed, and air temperature measurements by the buoys with the NCEP–NCAR re-analysis indicates that they follow each other quite closely. Since the bandpass-filtered SST variance used

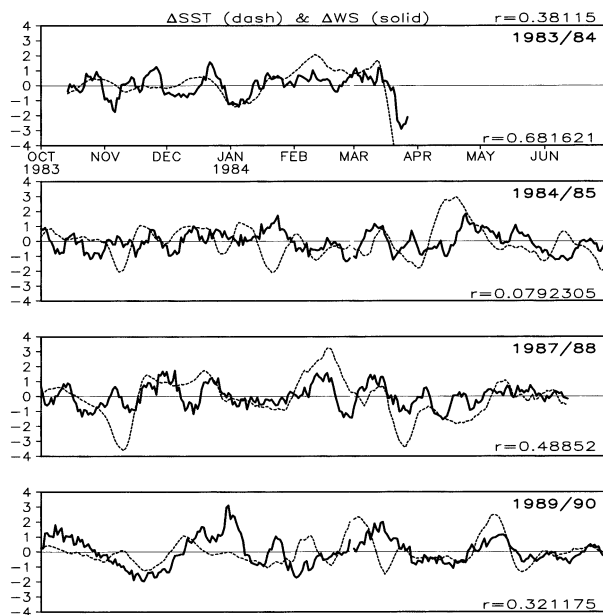


FIG. 4. Time series of 9 to 91 days bandpass-filtered differences of SST (dashed in  $^{\circ}\text{C}$ ) and surface wind speed (solid curves in  $\text{m s}^{-1}$ ) between buoy measurements and the concurrent NCEP–NCAR reanalysis. Correlation coefficient between SST and wind speed in each panel is shown at the lower-right corner.

in the NCEP–NCAR reanalysis is only 10% of that observed by buoys, we use the reanalysis wind data to track the intraseasonal variability that arises from internal chaotic dynamics of the atmosphere. To extract local SST-induced atmospheric variability, we subtract the reanalysis values from the buoy measurements and use the  $\Delta$  symbol to denote this difference. In our analysis of satellite data, this reference to reanalysis is not necessary since the intrinsic atmospheric variability has much larger scales than 1000 km and the extra zonal dimension afforded by satellite observations allows us to remove it effectively with a zonal filter.

Figure 4 shows the time series of  $\Delta\text{SST}$ s (dashed) and  $\Delta W$  (solid) for colder months of October–June, with  $W$  denoting wind speed. Except for 1984/85,  $\Delta\text{SST}$  and  $\Delta W$  are positively correlated. The  $\Delta\text{SST}$ – $\Delta W$  correlation amounts to 0.38 for the whole record shown in Fig. 4, significant at the 95% level. Here, the degree of freedom is estimated from the zero-crossing timescale of lagged SST autocorrelation. Similar significant correlation ( $r = 0.3$ ) is obtained using air–sea temperature difference instead of SST. Since the former is a measure of static stability, this result supports the conclusion from satellite data analysis that the vertical mixing is the major mechanism for surface wind adjustment.

Figure 5 shows two histograms of  $\Delta W$  for SSTs above (white bars) and below (black bars) one standard deviation, respectively. They are similar in overall shape but clearly shifted along the  $\Delta W$  axis, with the warm histogram on the high-speed side, and vice versa, indicating that with warm (cool) SSTs  $\Delta W$  tend to be

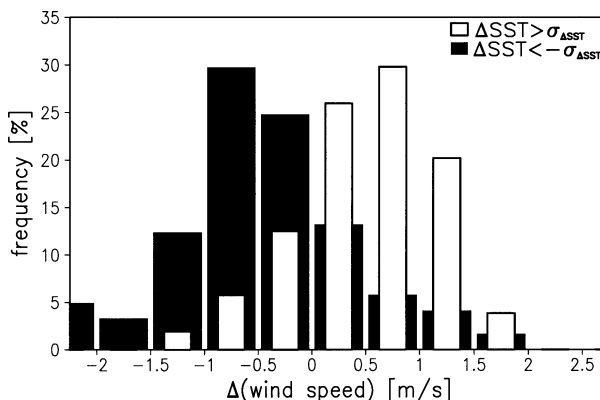


FIG. 5. Histograms of  $\Delta$ wind speed for  $\Delta\text{SST}$  above (white bars) and below (black bars) one standard deviation ( $\sigma$ ).

positive (negative). A Student's  $t$  test indicates that the means of two histograms are significantly different above the 90% confidence level. This corroborates the previous correlation analysis.

## 5. Kuroshio south of Japan

It is well known that the Kuroshio south of Japan does not have a unique path but varies between near-shore and offshore paths. Once the Kuroshio settles into one particular path, it tends to persist for months or even years. There is an extensive body of literature on the multipaths of the Kuroshio Current (see Kawabe 1995 for a review), but the exact physical mechanism for its path change remains unclear. Nonlinear dynamics of this strong current (e.g., Yamagata and Umatani 1989; Kubokawa 1989) and/or its interaction with eddies (Waseda et al. 2002) are generally believed to be important. The offshore paths are further divided into large-meander (LM) and non-LM types. The LM type is generally more persistent with a large offshore excursion of the Kuroshio axis (Kawabe 1995). In the following, we examine only the non-LM type of offshore paths since the LM type took place only once in late 1980s during our analysis period.

The Kuroshio south of Japan can be easily tracked in satellite SST imageries, where it appears as a streak of warm water. The core of maximum SST becomes blurred east of Japan. The Kuroshio took a nearshore path in 1998 and the TMI image shows the warm current hugging the south coast of Japan (Fig. 6a). In 2001, by contrast, the Kuroshio was in an offshore path and in Fig. 6b, the warm streak excurses from the coast for as far as 400 km around  $139^{\circ}\text{E}$ .

The TMI wind speed measurements reveal a remarkable association with the Kuroshio. Wind speed maximum tends to be located right on top of this warm current (Figs. 6c,d), a tendency especially clear in 2001 when the streaks of maximum SST and wind speed are collocated off the coast from  $135^{\circ}$  to  $140^{\circ}\text{E}$ . In addition,

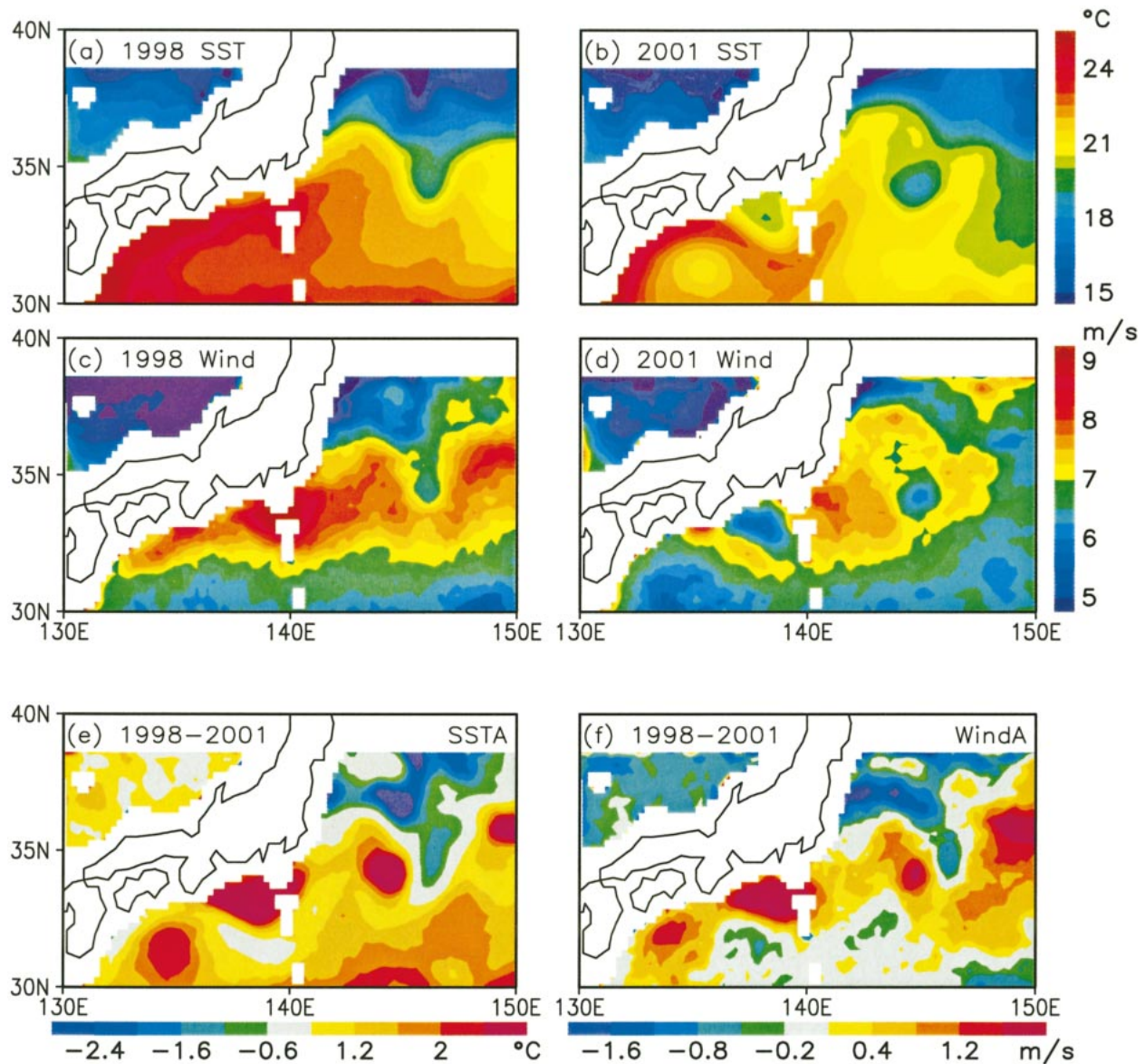


FIG. 6. Apr–Jun mean (a) 1998 and (b) 2001 SST, and (c) 1998 and (d) 2001 surface wind speed. The 1998 minus 2001 differences in (e) SST and (f) wind speed. Both SST and wind speed are observed by the TMI.

a local wind speed minimum is identifiable over a pinched-off cold ring centered at  $34^{\circ}\text{N}$ ,  $145^{\circ}\text{E}$  in 2001.<sup>1</sup> This SST–wind association is even better illustrated by the 1998 minus 2001 difference fields (Figs. 6e,f). With-out exception, each of the four major positive SSTA centers along the Kuroshio is collocated with a local enhancement of wind speed. SST-induced wind speed anomalies ( $\sim 1.6 \text{ m s}^{-1}$ ) are about 20% of the seasonal-

mean values ( $\sim 8 \text{ m s}^{-1}$ ) but are nevertheless apparent in the 2001 total field<sup>2</sup> (Fig. 6d).

In contrast to positive SST–wind correlation over the Kuroshio, positive SSTAs outside this strong current tend to be associated with reduced wind speed, for example, in the southern part of the domain and the Japan Sea (Figs. 6e,f). This negative correlation is indicative

<sup>1</sup> It recently came to our attention that similar ocean eddy–wind coupling is observed in the Gulf Stream region (Park and Cornillon 2002).

<sup>2</sup> We choose the April–June season for analysis here, the time when the climatological wind speed field reaches a broad meridional maximum over the Kuroshio. Because of weak gradients in the background, wind variations associated with changes in the Kuroshio path become readily visible.

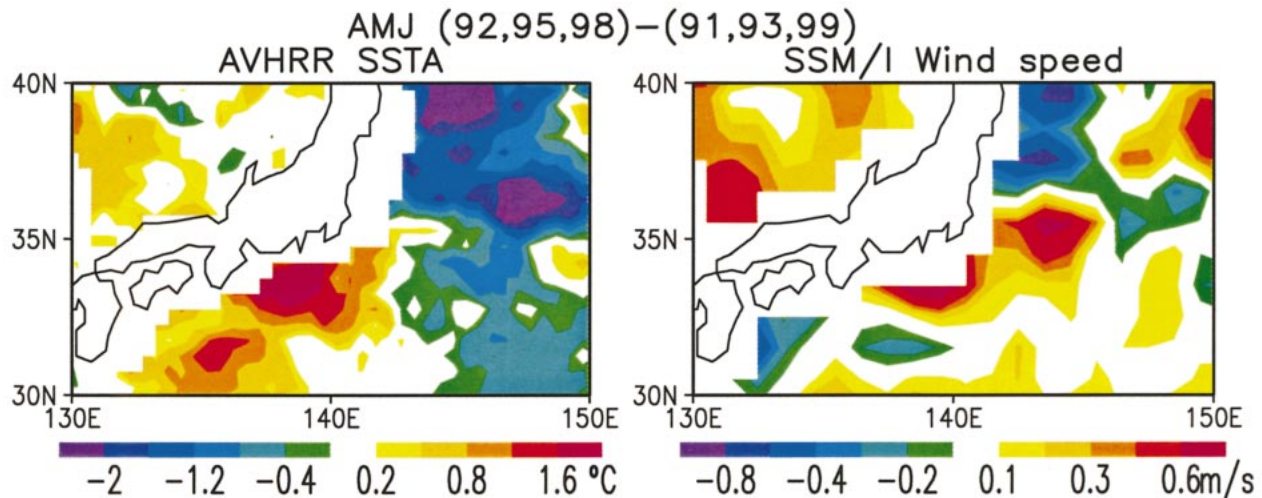


FIG. 7. Apr–Jun mean differences in (left) SST and (right) surface wind speed between years when the Kuroshio is in nearshore (1992, 1995, 1998) and offshore (1991, 1993, 1999) paths. AVHRR SST and SSM/I wind speed products are used.

of wind forcing of SST changes through surface turbulence heat flux and entrainment of cold subsurface water by oceanic mixing, a relation well known over the midlatitude central and eastern North Pacific with slack ocean current.

AVHRR SST and SSM/I wind velocity offer independent observations back to the late 1980s, albeit with somewhat degraded sampling. Figure 7 shows the composite difference fields between three nearshore and three offshore path years. Except south of Shikoku Island west of 135°E, SST and wind anomalies are still generally positively correlated along the Japanese coast. In particular, the large positive SSTAs around 140°E are associated with a wind speed increase. Thus we would conclude that the Kuroshio influence on surface wind is not limited to the recent period of TMI observations, but is a general feature of ocean–atmosphere interaction in this region.

## 6. Summary

Using satellite measurements, covariability in SST and surface wind speed is detected over the Kuroshio south of Japan and the KE region to the east, with high (low) wind speed found over warm (cool) SSTs. This SST–wind covariability is further confirmed by our analysis of in situ buoy measurements in the KE region. The KE region is also well known for atmospheric storm genesis. As a measure of internal chaos of the atmosphere, the standard deviation of intraseasonal (10–90 days) wind variability is  $1.3 \text{ m s}^{-1}$  based on our buoy data. In comparison, the standard deviation of SST-induced wind anomalies is  $0.3 \text{ m s}^{-1}$ . The detection of this modest SST effect amid high weather noise is made possible here by using an appropriate filter in space or time. In late spring and early summer, however, the close association between the Kuroshio south of Japan and

wind becomes readily visible even without such a filter (Fig. 6) because of reduced weather noise and favorable shifts in background fields.

The positive SST–wind speed correlation we observe over the Kuroshio and its extension is consistent with the vertical mixing adjustment to changing SST, a mechanism extensively studied for TIWs (Hayes et al. 1989; Xie et al. 1998; Liu et al. 2000; Chelton et al. 2001) and confirmed by shipboard vertical soundings (Hashizume et al. 2002). Similar SST-induced wind variations are observed farther upstream of the Kuroshio in the East China Sea (Xie et al. 2002), in the western Arabian Sea (G. Vecchi 2001, personal communication), and in the Southern Ocean (O’Neill et al. 2003). The characteristic positive correlation between anomalies of SST and wind speed is in sharp contrast with the negative one often observed on the basin scale in the extratropical Pacific (Namias and Cayan 1981; Frankignoul 1985) and Atlantic<sup>3</sup> (Wallace et al. 1990) that is indicative of atmosphere-to-ocean forcing. The positive SST–wind speed correlation reported in this paper indicates an opposite causality; as the strong Kuroshio Current meanders, the resultant SST anomalies cause the surface wind to change.

The Kuroshio–Oyashio Extension (KOE) is where the ocean memory of past wind changes is retrieved and affects SST changes. Xie et al. (2000) demonstrate this memory in an ocean GCM simulation forced by observed interannual wind stresses but without anomalous atmospheric thermal forcing. Large dynamically induced SST variance is found only in KOE over the off-equatorial North Pacific. This KOE memory is at the

<sup>3</sup> In the Tropics, however, such a negative SST–wind speed correlation may be indicative of two-way ocean–atmosphere interaction through latent heat flux (Okumura et al. 2001; Tanimoto and Xie 2002).

heart of Latif and Barnett's (1994) scenario of Pacific Decadal Oscillation. As North Pacific winds change, ocean Rossby waves are excited and propagate westward, causing changes in the KOE (Deser et al. 1999; Schneider and Miller 2001; Seager et al. 2001). Anomalous advection of temperature in the deep winter mixed layer leads to large SST anomalies there (Qiu 2002; Tomita et al. 2002). It is conceivable that these dynamically induced SST anomalies in the KOE will cause wind variations by the same mechanism as described in this paper. A recent study further suggests that via near-surface baroclinicity, KE variability can affect the Pacific storm track (Inatsu et al. 2002).

Our results reveal a new aspect of air–sea interaction in the KE region. The positive SST–wind speed correlation suggests a negative thermal feedback on SST; higher winds over positive SSTAs release more sensible and latent heat from the ocean, acting to reduce the SSTAs. The strength of this negative feedback depends on how the atmospheric boundary layer adjusts to changing SST as discussed in Frankignoul et al. (1998). The dynamic feedback of wind is not immediately clear at this time, but changes in Ekman pumping are likely to be large given the small horizontal scales (a few hundred kilometers) of wind anomalies. The combined thermal and dynamic feedback almost certainly affects SST and mixed layer depth in KE, which is the source region for the North Pacific Subtropical Mode Water characterized by its low potential vorticity (e.g., Suga and Hanawa 1995). Through the subduction process, these changes in KE may propagate further southward on isopycnal surfaces in the thermocline by passive advection (Hanawa and Kamada 2001) and via a dynamic adjustment that involves the potential vorticity minimum (Kubokawa and Xie 2002).

*Acknowledgments.* We would like to thank Jan Hafner for data preparation, B. Qiu, Y. Tanimoto, J. P. McCreary, H. Mitsudera, T. Endoh for valuable discussions, C. Frankignoul and an anonymous reviewer for detailed comments. The TMI and SSM/I data are obtained via ftp from Remote Sensing Systems, the QuikSCAT data from Physical Oceanography Distributed Active Archive Center of the Jet Propulsion Laboratory (JPL), and the ERS data from Institut Francais de Recherche pour l'Exploitation de la Mer. The SSH products are produced by the Space Oceanography Division of the Collecte Localisation Satellites, France. This study is supported by the Frontier Research System for Global Change, NASA through its JPL Contract 1216010 and Grant NAG5-10045, and the National Science Foundation of China (40240420564). The International Pacific Research Center is partly supported by the Frontier Research System for Global Change.

#### REFERENCES

- Alexander, M. A., I. Blade, M. Newman, J. R. Lanzante, N.-C. Lau, and J. D. Scott, 2002: The atmospheric bridge: The influence of

- ENSO teleconnections on air–sea interaction over the global oceans. *J. Climate*, **15**, 2205–2231.
- Cayan, D. R., 1992: Latent and sensible heat flux anomalies over the northern oceans: Driving the sea surface temperature. *J. Phys. Oceanogr.*, **22**, 859–881.
- Chelton, D. B., and Coauthors, 2001: Observations of coupling between surface wind stress and sea surface temperature in the eastern tropical Pacific. *J. Climate*, **14**, 1479–1498.
- Czaja, A., and C. Frankignoul, 1999: Influence of the North Atlantic SST on the atmospheric circulation. *Geophys. Res. Lett.*, **26**, 2969–2972.
- Deser, C., M. A. Alexander, and M. S. Timlin, 1999: Evidence for a wind-driven intensification of the Kuroshio Current extension from the 1970s to the 1980s. *J. Climate*, **12**, 1697–1706.
- Ducet, N., P. Y. Le Traon, and G. Reverdin, 2000: Global high-resolution mapping of ocean circulation from TOPEX/Poseidon and ERS-1 and -2. *J. Geophys. Res.*, **105**, 19 477–19 498.
- Frankignoul, C., 1985: Sea surface temperature anomalies, planetary waves, and air–sea feedback in the middle latitudes. *Rev. Geophys.*, **23**, 357–390.
- , A. Czaja, and B. L'Heveder, 1998: Air–sea feedback in the North Atlantic and surface boundary conditions for ocean models. *J. Climate*, **11**, 2310–2324.
- Hanawa, K., and J. Kamada, 2001: Variability of core layer temperature (CLT) of the North Pacific subtropical mode water. *Geophys. Res. Lett.*, **28**, 2229–2232.
- Hashizume, H., S.-P. Xie, W. T. Liu, and K. Takeuchi, 2001: Local and remote atmospheric response to tropical instability waves: A global view from space. *J. Geophys. Res.*, **106D**, 10 173–10 185.
- , —, M. Fujiwara, M. Shiotani, T. Watanabe, Y. Tanimoto, W. T. Liu, and K. Takeuchi, 2002: Direct observations of atmospheric boundary layer response to SST variations associated with Tropical instability waves over the eastern equatorial Pacific. *J. Climate*, **15**, 3379–3393.
- Hayes, S. P., M. J. McPhaden, and J. M. Wallace, 1989: The influence of sea-surface temperature on surface wind in the eastern equatorial Pacific: Weekly to monthly variability. *J. Climate*, **2**, 1500–1506.
- Hurlburt, H. E., A. J. Wallcraft, W. J. Schmitz, P. J. Hongan, and E. J. Metzger, 1996: Dynamics of the Kuroshio/Oyashio Current system using eddy-resolving models of the North Pacific Ocean. *J. Geophys. Res.*, **101**, 941–976.
- Inatsu, M., H. Mukougawa, and S.-P. Xie, 2002: Tropical and extratropical SST effects on the midlatitude storm track. *J. Meteor. Soc. Japan*, **80**, 1069–1076.
- Kalnay, E., and Coauthors, 1996: The NCEP/NCAR 40-Year Reanalysis Project. *Bull. Amer. Meteor. Soc.*, **77**, 437–471.
- Kawabe, M., 1995: Variations of current path, velocity, and volume transport of the Kuroshio in relation with the large meander. *J. Phys. Oceanogr.*, **25**, 3103–3117.
- Kubokawa, A., 1989: Growing solitary disturbance in a baroclinic boundary current. *J. Phys. Oceanogr.*, **19**, 182–192.
- , and S.-P. Xie, 2002: On steady response of a ventilated thermocline to enhanced Ekman pumping. *J. Oceanogr.*, **58**, 565–575.
- Latif, M., and T. P. Barnett, 1994: Causes of decadal climate variability over the North Pacific and North America. *Science*, **266**, 634–637.
- Liu, W. T., 2002: Progress in scatterometer application. *J. Oceanogr.*, **58**, 121–136.
- , X. Xie, P. S. Polito, S.-P. Xie, and H. Hashizume, 2000: Atmospheric manifestation of tropical instability waves observed by QuikSCAT and Tropical Rain Measuring Mission. *Geophys. Res. Lett.*, **27**, 2545–2548.
- Mizuno, K., and W. B. White, 1983: Annual and interannual variability in the Kuroshio Current System. *J. Phys. Oceanogr.*, **13**, 1847–1867.
- Namias, J., and D. R. Cayan, 1981: Large-scale air–sea interactions and short period climate fluctuations. *Science*, **214**, 869–876.

- Okumura, Y., S.-P. Xie, A. Numaguchi, and Y. Tanimoto, 2001: Tropical Atlantic air–sea interaction and its influence on the NAO. *Geophys. Res. Lett.*, **28**, 1507–1510.
- O’Neill, L. W., D. B. Chelton, and S. K. Esbensen, 2003: Observations of SST-induced perturbations of the wind stress field over the Southern Ocean on seasonal timescales. *J. Climate*, in press.
- Park, K.-A., and P. C. Cornillon, 2002: Stability-induced modification of sea surface winds over Gulf Stream rings. *Geophys. Res. Lett.*, **29**, 2211, doi:10.1029/2001GL014236.
- Qiu, B., 1995: Variability and energetics of the Kuroshio Extension and its recirculation gyre from the first two-year TOPEX data. *J. Phys. Oceanogr.*, **25**, 1827–1842.
- , 2002: The Kuroshio Extension system: Its large-scale variability and role in the midlatitude ocean–atmosphere interaction. *J. Oceanogr.*, **58**, 57–75.
- , K. A. Kelly, and T. M. Joyce, 1991: Mean flow and variability in the Kuroshio Extension from Geosat altimetry data. *J. Geophys. Res.*, **96**, 18 491–18 507.
- Robinson, W. A., 2000: Review of WETS—The Workshop on Extra-Tropical SST anomalies. *Bull. Amer. Meteor. Soc.*, **81**, 567–577.
- Schneider, N., and A. J. Miller, 2001: Predicting western North Pacific Ocean climate. *J. Climate*, **14**, 3997–4002.
- Seager, R., K. Kushnir, N. H. Naik, M. A. Cane, and J. Miller, 2001: Wind-driven shifts in the latitude of the Kuroshio–Oyashio Extension and generation of SST anomalies on decadal timescales. *J. Climate*, **14**, 4249–4265.
- Suga, T., and K. Hanawa, 1995: The subtropical mode water circulation in the North Pacific. *J. Phys. Oceanogr.*, **25**, 958–970.
- Tai, C. K., and W. White, 1990: Eddy variability in the Kuroshio Extension as revealed by Geosat altimetry: Energy propagation away from the jet, Reynolds stress, and seasonal cycle. *J. Phys. Oceanogr.*, **20**, 1761–1777.
- Tanimoto, Y., and S.-P. Xie, 2002: Inter-hemispheric decadal variations in SST, surface wind, heat flux and cloud cover over the Atlantic Ocean. *J. Meteor. Soc. Japan*, **80**, 1199–1219.
- Toba, Y., and H. Murakami, 1998: Unusual behavior of the Kuroshio Current system from winter 1996 to summer 1997 revealed by ADEOS-OCTS and other data—Suggestion of topographically forced alternating-jet instability. *J. Oceanogr.*, **54**, 465–478.
- Tomita, T., S.-P. Xie, and M. Nonaka, 2002: Estimates of surface and subsurface forcing for decadal sea-surface temperature variability in the mid-latitude North Pacific. *J. Meteor. Soc. Japan*, **80**, 1289–1300.
- Vazquez, J., K. Perry, and K. Kilpatrick, 1998: NOAA/NASA AVHRR oceans pathfinder sea surface temperature data set user’s reference manual. Tech. Rep. D-14070, Jet Propulsion Laboratory, Pasadena, CA, 82 pp.
- Wallace, J. M., C. Smith, and Q. Jiang, 1990: Spatial patterns of atmosphere–ocean interaction in the northern winter. *J. Climate*, **3**, 990–998.
- Waseda, T., H. Mitsudera, B. Taguchi, and Y. Yoshikawa, 2002: On the eddy–Kuroshio interaction: Evolution of the mesoscale eddies. *J. Geophys. Res.*, **107**, 3088, doi:10.1029/2000JC000756.
- Wentz, F. J., C. Gentemann, D. Smith, and D. Chelton, 2000: Satellite measurements of sea surface temperature through clouds. *Science*, **288**, 847–850.
- Wyrtki, K., L. Magaard, and J. Hagar, 1976: Eddy energy in the oceans. *J. Geophys. Res.*, **81**, 2641–2646.
- Xie, S.-P., M. Ishiwatari, H. Hashizume, and K. Takeuchi, 1998: Coupled ocean–atmospheric waves on the equatorial front. *Geophys. Res. Lett.*, **25**, 3863–3866.
- , T. Kunitani, A. Kubokawa, M. Nonaka, and S. Hosoda, 2000: Interdecadal thermocline variability in the North Pacific for 1958–97: A GCM simulation. *J. Phys. Oceanogr.*, **30**, 2798–2813.
- , W. T. Liu, Q. Liu, and M. Nonaka, 2001: Far-reaching effects of the Hawaiian Islands on the Pacific ocean–atmosphere. *Science*, **292**, 2057–2060.
- , J. Hafner, Y. Tanimoto, W. T. Liu, H. Tokinaga, and H. Xu, 2002: Bathymetric effect on the winter sea surface temperature and climate of the Yellow and East China Seas. *Geophys. Res. Lett.*, **29**, 2228, doi:10.1029/2002GL015884.
- Yamagata, T., and S.-I. Umatani, 1989: Geometry-forced coherent structures as a model of the Kuroshio large meander. *J. Phys. Oceanogr.*, **19**, 130–138.